Title

HIF2α-arginase axis is essential for the development of pulmonary hypertension.

Journal

Proceedings of the National Academy of Sciences of USA, 113(31)

Authors

Cowburn, Andrew
Crosby, Alexi
Macias, David
et al.

Publication Date

2016-08-02

DOI

10.1073/pnas.1602978113

Peer reviewed

HIF2α–arginase axis is essential for the development of pulmonary hypertension

Andrew S. Cowburn[a,b,1], Alexi Crosby[b], David Macias[a], Cristina Branco[a], Renato D. D. R. Colaço[a], Mark Southwood[c], Mark Toshner[b], Laura E. Crotty Alexander[d], Nicholas W. Morrell[b], Edwin R. Chilvers[b], and Randall S. Johnson[a,e,1]

[a]Department of Physiology, Development and Neuroscience, University of Cambridge, Cambridge CB2 3EG, United Kingdom; [b]Department of Medicine, University of Cambridge, Cambridge CB2 2QQ, United Kingdom; [c]Department of Pathology, Papworth Hospital National Health Service Foundation Trust, Cambridge CB23 3RE, United Kingdom; [d]Division of Pulmonary and Critical Care, School of Medicine, University of California, San Diego, La Jolla, CA 92093; and [e]Department of Cell and Molecular Biology, Karolinska Institute, Stockholm SE-171 77, Sweden

Edited by Gregg L. Semenza, Johns Hopkins University School of Medicine, Baltimore, MD, and approved June 10, 2016 (received for review February 22, 2016)

Hypoxic pulmonary vasoconstriction is correlated with pulmonary vascular remodeling. The hypoxia-inducible transcription factors (HIFs) HIF-1α and HIF-2α are known to contribute to the process of hypoxic pulmonary vascular remodeling; however, the specific role of pulmonary endothelial HIF expression in this process, and in the physiological process of vasoconstriction in response to hypoxia, remains unclear. Here we show that pulmonary endothelial HIF-2α is a critical regulator of hypoxia-induced pulmonary arterial hypertension. The rise in right ventricular systolic pressure (RVSP) normally observed following chronic hypoxic exposure was absent in mice with pulmonary endothelial HIF-2α deletion. The RVSP of mice lacking HIF-2α in pulmonary endothelium after exposure to hypoxia was not significantly different from normoxic WT mice and much lower than the RVSP values seen in WT littermate controls and mice with pulmonary endothelial deletion of HIF-1α exposed to hypoxia. Endothelial HIF-2α deletion also protected mice from hypoxia remodeling. Pulmonary endothelial deletion of arginase-1, a downstream target of HIF-2α, likewise attenuated many of the pathophysiological symptoms associated with hypoxic pulmonary hypertension. We propose a mechanism whereby chronic hypoxia enhances HIF-2α stability, which causes increased arginase expression and dysregulates normal vascular NO homeostasis. These data offer new insight into the role of pulmonary endothelial HIF-2α in regulating the pulmonary vascular response to hypoxia.

pulmonary | hypertension | hypoxia | HIF

Alveolar hypoxia affects vascular flow in the pulmonary vascular bed via an immediate vasoconstrictor response (hypoxic pulmonary vasoconstriction, or HPV) (1). This reduces perfusion of regions of the lung with lowered levels of airflow (2). In conditions including chronic obstructive pulmonary disease (3), idiopathic pulmonary fibrosis (4), and at high altitude (5), HPV probably contributes to persistent increases in pulmonary arterial pressures. This in turn is correlated with reduced plasticity of the vascular bed, sustained pulmonary vascular remodeling, and, ultimately, debilitating right ventricular hypertrophy (RVH) and failure (2).

The hypoxia-inducible factors (HIFs) are transcription factors and key regulators of the molecular response to hypoxia. The targets of HIFs include genes controlling vascularization, cellular proliferation, migration, and metabolism (6–11). A well-characterized animal model of hypoxia-induced pulmonary hypertension involves exposure to chronic hypoxia (CH), typically 10–12% inspired oxygen. This results in extensive vascular remodeling, marked pulmonary hypertension and RVH over a period of a few weeks. Exposure to CH in rodents results in vasoconstriction and a pattern of vascular remodeling that is reminiscent of humans with hypoxia-associated pulmonary hypertension (12, 13).

Mice that are hemizygous for either of the HIF isoforms, HIF-1α (14) or HIF-2α (15), have been shown to have attenuated pulmonary vascular remodeling following experimental CH. Conditional deletion of HIF-1α in smooth muscle also ameliorates the degree of remodeling in CH (16). The mechanisms by which HIF acts in pulmonary vascular remodeling are not fully defined; in particular, the role played by the endothelium in this process is not well understood. Here, we delete the HIF isoforms and one of their targets, the Arginase-1 (*Arg1*) gene, specifically in the pulmonary endothelium (17), and show that expression of the HIFα transcription factors in pulmonary endothelial cells is an essential aspect of the hypoxic response of the lung.

Results

Deletion of HIFα Isoforms in Pulmonary Endothelium. Genetically manipulated mouse strains with conditional alleles of either the HIF-1α or -2α isoforms (18, 19) were crossed to mouse strains expressing the cre recombinase enzyme under the control of the pulmonary endothelium-specific Alk1- or L1 promoter (L1cre) (17). To determine tissue specificity of this transgene, we analyzed the cre activity of adult L1cre mice by crossing with a ROSA26Sor$^{tm9(CAG\text{-}tdTomato)}$ reporter strain. As shown, lung vasculature was easily identifiable. Minimal expression of tdTomato was detectable in the endothelium of other tissues (Fig. S1*A*). Deletion efficiency was assessed and deletion was greater than 80% (Fig. S1*B*), with little or no detectable deletion in other tissues.

HIF-2α Deletion in the Pulmonary Endothelium Prevents Hypoxia-Induced Pulmonary Hypertension. WT and pulmonary endothelial HIF-α deleted mice were exposed to normoxic or hypoxic (10% O_2) normobaric atmospheres for 21 d. Pulmonary hypertension was assessed through measurement of right ventricular systolic pressures (RVSPs) (Fig. 1*A*). RVSPs in L1cre-HIF-2α mice (18.9 ± 1.0 mmHg, $n = 11$) under normoxic conditions were significantly lower than in littermate controls (22.4 ± 1.1 mmHg, $n = 9$, $P = 0.03$) mice. However, RVSPs from normoxic L1cre-HIF-1α mice (24.7 ± 1.7 mmHg, $n = 6$) did not differ from those of WT controls (Fig. 1*A*).

Significance

The expression of hypoxia-inducible factor (HIF)-2α in pulmonary endothelium of mice influences pulmonary vascular resistance and development of hypoxic pulmonary hypertension (PH) via an arginase-1–dependent mechanism. The HIF-2α:arginase-1 axis influences the homeostatic regulation of nitric oxide synthesis in the lung. Impaired generation of this vasoactive agent contributes to the initial development and vascular remodeling process of PH.

Author contributions: A.S.C., C.B., N.W.M., E.R.C., and R.S.J. designed research; A.S.C., A.C., D.M., C.B., R.D.D.R.C., M.S., M.T., L.E.C.A., and N.W.M. performed research; A.S.C., E.R.C., and R.S.J. analyzed data; and A.S.C., E.R.C., and R.S.J. wrote the paper.

The authors declare no conflict of interest.

This article is a PNAS Direct Submission.

Freely available online through the PNAS open access option.

[1]To whom correspondence may be addressed. Email: asc32@medschl.cam.ac.uk or rsj33@cam.ac.uk.

This article contains supporting information online at www.pnas.org/lookup/suppl/doi:10.1073/pnas.1602978113/-/DCSupplemental.

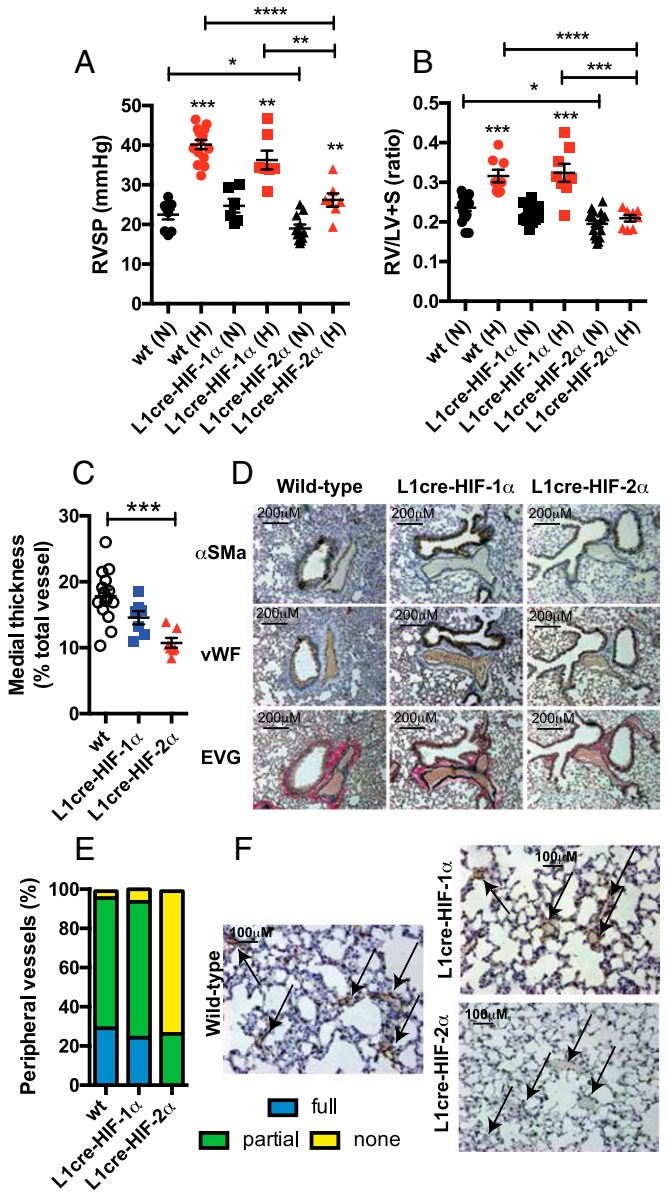

Fig. 1. Pulmonary endothelial HIF-2α contributes to chronic hypoxic pulmonary hypertension. (*A*) Scatter plot (mean ± SEM) of RVSP. WT and L1cre-HIFα mice were housed in normoxia (N) or CH (H) [WT (N) $n = 9$, (H) $n = 12$; L1cre-HIF-1α (N) $n = 6$, (H) $n = 7$; L1cre-HIF-2α (N) $n = 11$, (H) $n = 7$]. (*B*) RVH. Scatter plot (mean ± SEM) shows RV/LV+S weight ratio in mice exposed to normoxia (N) or CH (H) [WT (N) $n = 9$, (H) $n = 12$; L1cre-HIF-1α (N) $n = 6$, (H) $n = 7$; L1cre-HIF-2α (N) $n = 11$, (H) $n = 7$]. (*C* and *D*) Airway remodeling in WT ($n = 15$), L1cre-HIF-1α ($n = 7$), and L1cre-HIF-2α ($n = 7$) postchronic hypoxic challenge. (*C*) Scatter plot (mean ± SEM) of pulmonary vessel medial thickness. Quantification of the intimal medial thickness achieved by staining lung sections with elastic van Gieson (EVG). (*D*) Histological sections immunostained with α-SMA, von Willebrand factor (vWF), and EVG. Representative photomicrographs demonstrate lack of remodeling in L1cre-HIF-2α pulmonary arteries associated with terminal bronchi. Loss of HIF-2α in pulmonary endothelial cells reduces the degree of muscularization of peripheral arteries. (Scale bars, 200 μM.) (*E*) Stacked bar chart showing muscularization of peripheral pulmonary arteries in lung sections (blue bar, full muscle ring; green bar, partial muscle ring; and yellow bar, no muscle ring) from WT ($n = 15$), L1cre-HIF-1α ($n = 9$), and L1cre-HIF-2α ($n = 7$) mice. (*F*) Representative photomicrographs immunostained for α-smooth muscle (arrows point to distal vessels). (Scale bars, 100 μM.) $^*P < 0.05$, $^{**}P < 0.001$, $^{***}P < 0.0001$.

The RVSPs of L1cre-HIF-2α mice following hypoxic exposure (26.1 ± 1.6 mmHg, $n = 7$) were not significantly different from those of untreated WT mice (22.48 ± 1.19, $n = 9$) and were much lower than the elevated values seen in WT littermate controls (41.9 ± 1.8 mmHg, $n = 12$, $P < 0.0001$) and L1cre-HIF-1α mice (36.25 ± 2.37 mmHg, $n = 7$, $P < 0.005$) (Fig. 1*A*).

The ratio of right ventricular weights to those of the left ventricle plus septum (RV/LS+S), an indicator of RVH, was likewise significantly higher in WT (0.316 ± 0.01, $n = 8$, $P < 0.0001$) and L1cre-HIF-1α (0.323 ± 0.02, $n = 8$, $P < 0.001$) mice exposed to hypoxia compared with the ratios found in L1cre-HIF-2α (0.209 ± 0.008, $n = 8$) mice (Fig. 1*B*). WT and mutant mice reacted to hypoxia normally in other respects (Fig. S2 *A–C*).

Pulmonary Endothelial HIF-2α Is Essential for Vascular Remodeling. Medial thickening of pulmonary vessels was calculated. Both WT littermates and L1cre-HIF-1α mice showed significantly increased medial thickness following hypoxic conditioning (Fig. 1*C*). In comparison, hypoxic L1cre-HIF-2α mice showed a large relative reduction in medial thickness relative to WT animals. Normoxic animals showed no changes in vessel structure (Fig. S3).

Serial lung sections were immunostained to mark endothelial cells. Lungs from WT and L1cre-HIF-1α mice had typical tissue remodeling following CH (Fig. 1*D*), with an increase in α-smooth muscle actin (α-SMA) associated with pulmonary arteries (Fig. 1*E*). However, little to no remodeling was observed in lung sections from L1cre-HIF-2α mice (Fig. 1*F*). Lung sections showed increases in elastin in both WT controls and L1cre-HIF-1α mice, but only minimal staining in the L1cre-HIF-2α mice (Fig. 1*D*) (20). Collagen was also significantly higher in hypoxia-conditioned WT and L1cre-HIF-1α mice relative to L1cre-HIF-2α mice (Fig. S4*A*). Pulmonary endothelial deletion of HIF-2α reduced smooth muscle cell coverage after hypoxic exposure (Fig. 1*F*). In comparison, both WT littermate control and L1cre-HIF-1α mice developed full and partial rings of α-SMA–positive cells around vessels in hypoxia-conditioned animals (Fig. 1*F*).

Reduced Arginase Expression in HIF2α Mutant Mice. Previous work from our laboratory and others has demonstrated that the two HIFα isoforms act to control NO homeostasis during hypoxia. This occurs through HIF1α regulation of the NOS2/iNOS gene, and HIF-2α regulation of the Arg-1 and Arg-2 genes (21–25). The enzyme Arg-2 in particular has been implicated in reducing airway NO and promoting remodeling and collagen deposition in pulmonary arterial hypertension (PAH) patients (26, 27). We found that hypoxic up-regulation of arg-1 and -2 was reduced in hypoxia-conditioned isolated murine primary pulmonary endothelial cells (Fig. S5*A*) and whole lung samples from L1cre-HIF-2α mice, relative to WT littermate controls following hypoxic conditioning (Fig. 2*A*).

Consistent with these data, we found that plasma $NO_{(X)}$ concentrations were significantly reduced in HIF-1α mice and elevated in HIF-2α mutant mice compared with WT control mice (Fig. 2*B*); this was mirrored in an increase in NO metabolites detected in whole lung extracts of hypoxically treated animals (Fig. 2*C*). There was also an increase in exhaled NO detected in HIF-2α mutant mice (Fig. 2*D*). Although several recent studies have highlighted the role of endothelin-1 (ET-1) in pulmonary hypertension and indicated its regulation by the HIF pathway, purified lung endothelial cells showed little change in ET-1 expression in this model (Fig. S5 *B–D*). There was a significant increase in PDGF-β expression in WT mice during the acute hypoxic phase (days1–3) before levels returned to near baseline at the chronic phase (day 21). However, there seems to be little separation between WT and L1cre-HIF2α mice (Fig. S6 *A–D*). We further analyzed a number of stem cell markers known to be up-regulated in PAH (28). We found enhanced whole lung gene expression of

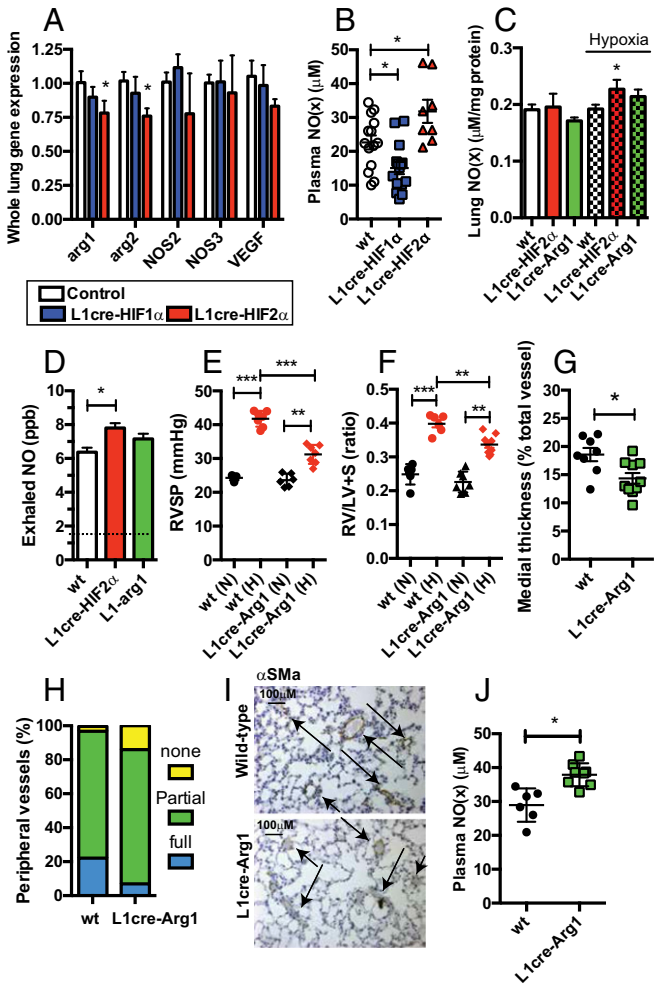

Fig. 2. Endothelial deletion of HIF-2α maintains higher plasma nitrate levels. (*A*) Quantitative PCR (qPCR) analysis of arginase-I/-II, NOS2, and VEGF mRNA from whole lung samples of WT (open bar, $n = 7$), L1cre-HIF-1α (blue bar, $n = 7$), and L1cre-HIF-2α (red bar, $n = 6$). (*B* and *C*) Total NO in (*B*) plasma and (*C*) whole lung by the conversion of $NO_{(X)}$ to NO using an NO analyzer (Sievers). Data shown as scatter plot with mean ± SEM from WT ($n = 7$), L1cre-HIF-1α ($n = 7$), and L1cre-HIF-2α ($n = 6$) after CH challenge. (*C*) Whole lung lysate analysis for $NO_{(X)}$ in normoxic WT (open bar, $n = 7$), L1cre-HIF2α (red bar, $n = 7$), and L1cre-Arg1 (green bar, $n = 4$) and following CH (10% O_2 21 d), WT (white checkered bar, $n = 16$), L1cre-HIF2α (red checkered bar, $n = 7$), and L1cre-Arg1 (green checkered bar, $n = 9$). (*D*) Exhaled NO was measured noninvasively in nonanesthetized mice. In normoxia gas phase NO was measured by a chemiluminescence-based NO analyzer (carrier gas baseline 1.7 ppb, dotted line). Data shown as bar graph with mean ± SEM for normoxic WT ($n = 13$), L1cre-HIF-2α ($n = 8$), and L1-Arg1($n = 5$). Pulmonary endothelial deletion of Arg-1 attenuates hypoxic pulmonary hypertensive phenotype. (*E*) Scatter plot (mean ± SEM) shows the effect of pulmonary endothelial Arg-1 on RVSP. WT and L1cre-Arg1 mice were housed in normoxia (N) or CH (H) [WT (N) $n = 5$, (H) $n = 7$; L1cre-Arg1 (N) $n = 6$, (H) $n = 7$]. (*F*) Effect of pulmonary endothelial Arg-1 on RVH. Scatter plot (mean ± SEM) shows RV/LV+S weight ratio in mice exposed to normoxia (N) or CH (H) [WT (N) $n = 6$, (H) $n = 6$; L1cre-Arg1 (N) $n = 7$, (H) $n = 9$]. (*G*) Airway remodeling was determined in WT ($n = 8$) and L1cre-Arg1 ($n = 10$). Quantification of the intimal medial thickness. (*H*) Stacked bar chart showing the degree of muscularization of peripheral pulmonary arteries in lung sections from WT ($n = 5$) and L1cre-Arg1 ($n = 6$) mice. (*I*) Representative photomicrographs immunostained for α-SMA showing near and complete ring formation in peripheral vessel of WT mice compared with L1cre-Arg1 mice. (Scale bars, 100 μM.) (*J*) Total NO was determined in the plasma by the conversion of NO_x to NO using an NO analyzer (Sievers). Data shown as scatter plot with mean ± SEM from WT ($n = 6$) and L1cre-Arg1 ($n = 8$) after CH challenge. *$P < 0.05$, **$P < 0.001$, ***$P < 0.0001$.

both Oct3-4 and nanog in WT compared with L1cre-HIF2α mice (Fig. S6 *E–H*).

Pulmonary Endothelial Arginase-1 Deletion Attenuates PAH. We next sought to determine how the specific deletion of arginase-1 in the pulmonary endothelium influenced the development of PAH. The increase in RVSP normally observed following chronic hypoxic challenge (for WT mice, 41.7 ± 0.8 mm/Hg, $n = 7$, $P < 0.0001$) was significantly attenuated in mice with pulmonary endothelial arginase-1 deletion (31.2 ± 1.0 mmHg, $n = 7$) (Fig. 2*E*). Basal RVSPs in L1cre-arg1 mice under normoxia (23.0 ± 0.7 mmHg, $n = 6$) were similar to those seen in littermate WT control mice (24.3 ± 0.3 mmHg, $n = 5$). The RV/LS+S was significantly higher in WT (0.39 ± 0.01, $n = 6$, $P < 0.001$) compared with L1cre-arg1 (0.33 ± 0.01, $n = 9$) mice, following chronic hypoxic exposure (Fig. 2*F*); the animals otherwise responded normally to hypoxia (Fig. S7*A*). WT littermates showed significantly greater medial thickening (18.57%, $n = 15$) compared with L1cre-arg1 mice (14.35%, $n = 9$) after exposure to CH (Fig. 2*G*). Collagen deposition around the bronchial-associated vasculature was significantly higher in hypoxically conditioned WT control mice relative to L1cre-arg1 mice (Fig. S4*B*).

L1cre-arg1 mice showed substantially less α-SMA associated with pulmonary arteries in close proximity to terminal bronchioles compared with WT controls (Fig. S7*B*). Staining for α-SMA was also substantially reduced in the peripheral pulmonary vasculature of these mutants (Fig. 2 *H* and *I*). Deletion of pulmonary endothelial arg-1 significantly elevated plasma $NO_{(x)}$ relative to the levels seen in plasma from WT control mice (Fig. 2*J*).

Changes in Acute Response to Hypoxia Caused by Loss of Endothelial HIF-2α. Hypoxia rapidly stimulates pulmonary vascular resistance (HPV) and increases the pressure needed to maintain normal output from the right ventricle of the heart. We compared HPV in WT control and mutant animals by measuring RVSPs, both immediately before and during hypoxic challenge (method shown in Fig. 3*A*). L1cre-HIF-2α mice have a lower resting RVSP (18.99 ± 1.00 mmHg, $n = 11$) than WT control animals (22.47 ± 1.19 mmHg, $n = 9$) (Fig. 1*A*); nonetheless, the magnitude of pressure changes induced by hypoxia were still significantly lower in mice lacking pulmonary endothelial HIF-2α (3.10 ± 0.60 mmHg, $n = 13$) relative to that seen in WT animals (5.45 ± 0.76 mmHg, $n = 13$, $P = 0.023$). RVSP recorded from L1cre-HIF-1α (4.56 ± 1.53 mmHg, $n = 7$) mice, however, did not significantly deviate from WT controls (Fig. 3*B*) during acute hypoxic exposure. Thus, acute pressure changes in the pulmonary circulation induced by hypoxia are significantly lower in animals that lack HIF-2α in the pulmonary endothelium. Baseline arterial saturations for L1cre-HIF-2α mice did not deviate from WT controls (Fig. 3*C*). However, during the acute hypoxic challenge, there was a strong trend toward greater desaturation in the L1cre-HIF-2α compared with WT mice (Fig. 3*C*, $P = 0.06$, $n = 7$).

Whole-body plethysmography showed that resting ventilation rates in normoxia are similar in the HIFα mutant animals relative to WT controls [WT control 168 ± 3.0 breaths per minute (BrPM), L1cre-HIF-1α 174 ± 2.8 BrPM, and L1cre-HIF-2α 170 ± 2.7 BrPM] (Fig. 3*D*). All mice responded to acute hypoxia by increasing ventilation rates. L1cre-HIF-1α and WT littermate control mice increased to 258 and 250 BrPM, respectively, for the initial 5 min before reducing their ventilation rates to 187 and 174 BrPM during the first hour of exposure to hypoxia. However, L1cre-HIF-2α mice increased respiratory rate to 308 BrPM, then reduced their ventilation rates to 233 BrPM in the same time period (Fig. 3*D*). Of note, both tidal volume and peak inhalation/exhalation flow rates are comparable between the three groups (Fig. S8 *A–C*), indicating that there is no anatomic difference in pulmonary capacity. The carotid bodies in all animals were histologically normal (Fig. S8 *D–H*).

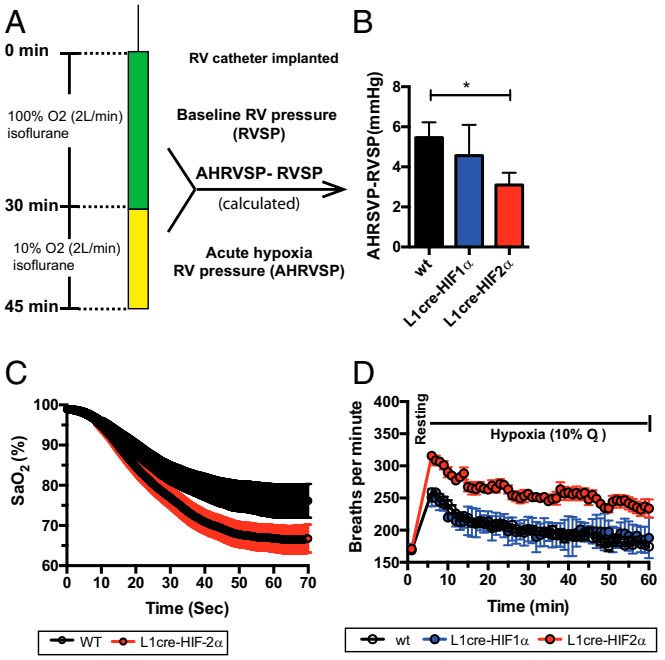

Fig. 3. Acute HPV is significantly blunt in L1cre-HIF-2α mutants. (*A*) Line diagram showing the time line and gas composition used to determine the acute HPV response. (*B*) Acute HPV was determined by measuring RVSP before and during acute hypoxic challenge (10% O_2). The delta between the two pressures was determined as the hypoxic vasoconstriction response. Data shown in bar graph as mean ± SEM from WT ($n = 13$), L1cre-HIF-1α ($n = 7$), and L1cre-HIF-2α ($n = 13$). (*C*) Percentage arterial oxygen saturation was recorded during the acute hypoxic challenge. Data recorded at 5-s intervals mean ± SEM of WT ($n = 7$) and L1cre-HIF-2α ($n = 7$). (*D*) Ventilation rate in response to acute hypoxia was determined by whole-body plethysmography. Resting/normoxic ventilation was determined 60 min before acute hypoxic stimulus. Data shown as mean BrPM ± SEM for WT ($n = 10$), L1cre-HIF-1α ($n = 5$), and L1re-HIF-2α ($n = 6$). *$P < 0.05$.

Endothelial Progenitor Cells from Human PAH Patients Have Altered HIF-2α–Dependent Arginase Expression. Blood outgrowth endothelial cells (BOECs) have been extensively used as a model for studying in vitro endothelial function in vascular disorders (29, 30) with close functional and gene expression similarity to pulmonary artery endothelial cells (31).

Previous work has shown enhanced expression and activity of Arg-2 in PAH patients (27, 32). Fig. 4*A* demonstrates that these cells have no deficiencies in HIF expression, and that Arg-2 expression is increased in the PAH patient-derived cells (Fig. 4*A* and Fig. S9 *A* and *B*). Hypoxia further increases the expression of Arg-2 in these BOECs from PAH patients.

BOECs from control volunteers produce significantly more NO than BOECs from PAH patients following 48 h in culture (Fig. S9*C*). NO production was restored to near that seen in control BOECs following arginase inhibition with *S*-(2-boronoethyl)-L-cysteine (BEC) (Fig. S9*C*). shRNA technology was used to specifically knock down HIF-1α, HIF-2α, and Arg-2 in these BOECs. These data show that knockdown of HIF-2α suppresses the expression of Arg-2 (Fig. 4*B*) and decreases Arg-2 enzyme activity in these cells from patients with PAH (Fig. 4*C*).

Discussion

In this study, we have shown that the endothelial cell is a necessary element in the changes that result in PAH, and that the HIF isoform HIF-2α is in turn required for that endothelial response. We also observed the down-regulated expression of arginase in isolated pulmonary endothelial cells and whole lungs from L1cre-HIF2a mice following CH and demonstrate here that deletion of arginase-1 specifically in the pulmonary endothelium attenuated the development of hypoxic pulmonary hypertension. Given the role of HIF-2α in regulating arginases specifically, this indicates that a key aspect of the function of HIF-2α in PAH is its regulation of arginase expression.

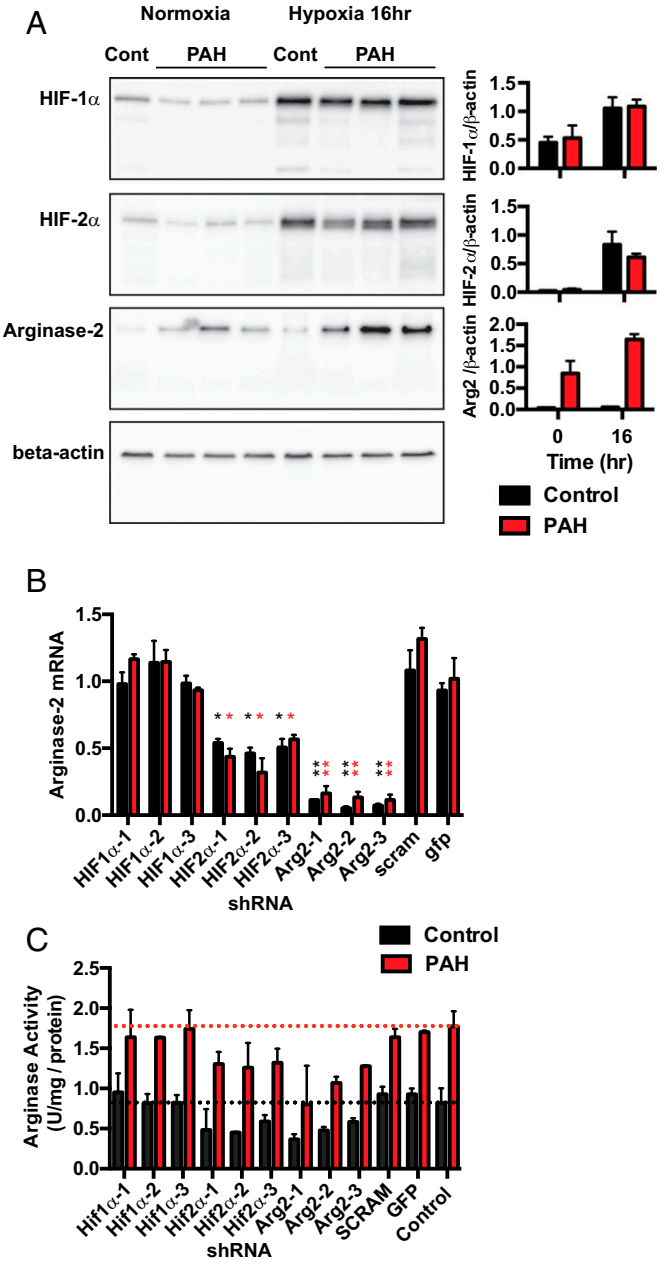

Fig. 4. Analysis of human BOECs as a model for studying in vitro endothelial function in PAH. (*A*) Western blot analysis of HIF1α and HIF2α stability and arginase-2 expression in normoxia and 16 h posthypoxia. Data shown in bar graph as a ratio of target gene to β-actin, mean ± SEM of control (closed bar, $n = 3$) and PAH (red bar, $n = 4$). (*B*) A lentiviral shRNA strategy was used to target HIF1α, HIF2α, and Arg-2 expression. Three shRNAs were used to knock down each gene of interest. A scramble short hairpin and GFP-tagged lentivirus and no treatment were included as controls. Data shown (mean ± SEM qPCR fold change compared with no-treatment control) for Arg-2 from control (black bar, $n = 3$) and PAH (red bar, $n = 3$) 16 h posthypoxia. (*C*) Cell lysates were analyzed for arginase activity following the shRNA strategy to knock down HIF1α, HIF2α, and Arg-2. Data are shown as mean ± SD of urea produced corrected per milligram of protein lysate for control (black bar $n = 2$) and PAH (red bar $n = 2$). *$P < 0.05$, **$P < 0.001$ (control) and *$P < 0.05$, **$P < 0.001$(PAH).

The HIF pathway was implicated in PH initially through demonstrations showing that mice hemizygous for HIF-1α or HIF-2α have diminished levels of pulmonary hypertension (15, 33); subsequent work was able to show that hemizygosity for HIF-1α resulted in changes in myocyte hypertrophy and polarization (14). In contrast, hemizygosity of HIF-2α revealed that endothelial changes resulting in PAH were partially blocked when HIF-2α was diminished (15). Recent studies have also shown that PHD2 loss, which gives rise to increased HIF protein stability, promotes an HIF-2α–dependent increase in pulmonary hypertension (34, 35). These studies further demonstrate the importance of the HIF pathway in the etiology of PAH.

The causal link between pulmonary hypertension and NO homeostasis has been extensively documented (26, 36), and this is reflected clinically in the finding that intrapulmonary nitrates, biochemical reaction products of NO in bronchoalveolar fluid, and exhaled NO are all diminished in human pulmonary hypertension (37, 38). Interestingly, primary pulmonary endothelial cells isolated from PAH patients have substantially increased expression of arg-2 (27), which would be predicted to decrease available L-arginine and reduce NOS-derived NO formation. We have previously shown that both Arg1 and Arg2 are HIF-2α–dependent genes, and we show here that their expression in pulmonary endothelium is decreased in HIF-2α pulmonary endothelium mutants. This should result in an increase in pulmonary endothelial NO, which itself has been shown to alleviate PAH experimentally (39). Consistent with this hypothesis, genetic deletion of arg-1 resulted in a marked attenuation in the pathologies associated with PAH. Given a mechanistic link between these findings and the etiology of PAH, future therapies to manipulate the control of NO homeostasis by the HIFα pathway should certainly be explored.

Methods

Animals. All animals were housed in a facility approved by the Association for Assessment and Accreditation of Laboratory Animal Care International. All protocols and surgical procedures were approved by the local and national animal care committees. Targeted deletion of HIF-1α, HIF-2α, and arginase-1 in pulmonary endothelial cells was created by crossing (C57Bl6/j) homozygous for the floxed allele in HIF-1α, HIF-2α, or arginase-1 into a background of Cre recombinase expression drive by the L1 (alk-1) promoter kindly donated by Paul Oh, University of Florida, Gainesville, FL (17). Mice characterized as WT were in all cases littermates of respective mutant mice, homozygous for conditional alleles but without the cre recombinase transgene.

Measurement of RVSP. For induction of PAH due to CH, groups of male mice (8–12 wk) were maintained in a normobaric hypoxic chamber (FiO_2 10%) for up to 21 d. Mice were weighed then anesthetized (isoflurane) and right-sided heart catheterization was performed through the right jugular using a pressure-volume loop catheter (Millar) (40–42). Blood was taken for hemodynamic assessment.

RVH. To measure the extent of RVH, the heart was removed and the right ventricule (RV) free wall was dissected from the left ventricle plus septum (LV+S), and weighed separately (43). The degree of RVH was determined from the ratio RV/LV+S.

Tissue Preparation. In all animals the left lung was fixed in situ in the distended state by the infusion of 0.8% agarose into the trachea and then placed in 10% (wt/vol) paraformaldehyde before paraffin embedding. The right lung was frozen in liquid nitrogen for mRNA extraction.

Pulmonary Vascular Morphometry. Detailed methods are given in *SI Methods*.

Hematological Analysis. Anticoagulated blood was analyzed using Vet abc hematology analyzer (Horiba) according to the manufacturer's instructions.

Nitrite/Nitrate Analysis. Blood samples were centrifuged to separate plasma and were passed through a column with a 10-kDa cutoff filter. All samples were analyzed for total $NO_{(X)}$ content using a NOA 280i (Sievers; GE Healthcare) according to the manufacturer's instructions.

RNA Analysis. Detailed methods are given in *SI Methods*.

BOEC isolation culture. BOECs have been extensively used as a model for studying in vitro endothelial function in vascular disorders (29, 30) and we have previously demonstrated their close functional and gene expression similarity to pulmonary artery endothelial cells (31). BOECs were isolated as previously described (44). BOECs were isolated from peripheral blood was taken from consenting healthy volunteers at the Addenbrooke's University of Cambridge teaching hospital National Health Service Foundation Trust, Cambridge, United Kingdom, following a protocol approved by the Cambridge Research Ethics Committee (REF:11/EE/0297). Detailed methods are given in *SI Methods*.

Arginase activity assay. BOECs were prepared in lysis buffer for an arginase activity assay as previously described (45). Detailed methods are given in *SI Methods*.

Carotid Body Histology. Carotid body histology was performed as previously reported (46). Carotid body volume and cell numbers were quantified on microscope images (Leica DM-RB) using ImageJ software. Detailed methods are given in *SI Methods*.

Whole-Body Unrestrained Plethysmography. A single-chamber plethysmograph (Data Science) was used in conjunction with a pressure transducer. Nonanesthetized mice were randomly placed into the plethysmograph and allowed to acclimate. Once they were acclimated to the chamber, the composition of the flow gas was switched from 21% O_2 to 10% O_2 using a PEGAS mixer (Columbus Instruments). Detailed methods are given in *SI Methods*.

Exhaled NO analysis. Exhaled NO was measured noninvasively in nonanesthetized mice using a closed chamber system as previously described (47). Briefly, gas phase NO was measured by a chemiluminescence-based NO analyzer sensitive to 0.1ppb NO (NOA 280i; Sievers). Detailed methods are given in *SI Methods*.

Primary lung endothelial cell isolation. Primary endothelial cells were isolated and cultured from lungs of L1cre-HIF2α and WT mice, as previously described (25). Detailed methods are given in *SI Methods*.

Knockdown experiments. Human BOECs derived from both control and PAH donors were transduced using lentiviral particles containing three different shRNAs targeting human HIF-1α, HIF-2α, and Arg-2 mRNA, respectively. Detailed methods are given in *SI Methods*.

Statistical Analysis. All data represents the mean (±SEM) of n separate experiments unless otherwise stated. Difference between groups was assessed using t test unless otherwise stated. A P value of <0.05 was considered significant.

ACKNOWLEDGMENTS. We thank Dr. Paul Oh (University of Florida) for providing the L1(alk-1)cre mouse. This study was funded by The Wellcome Trust, Papworth Hospital National Institute for Health Research Cambridge Biomedical Research Centre.

1. von Euler US, Liljestrand G (1946) Observations on the pulmonary arterial blood pressure in the cat. *Acta Physiol Scand* 12(4):301–320.
2. Sylvester JT, Shimoda LA, Aaronson PI, Ward JP (2012) Hypoxic pulmonary vasoconstriction. *Physiol Rev* 92(1):367–520.
3. Naeije R (2005) Pulmonary hypertension and right heart failure in chronic obstructive pulmonary disease. *Proc Am Thorac Soc* 2(1):20–22.
4. Lettieri CJ, Nathan SD, Barnett SD, Ahmad S, Shorr AF (2006) Prevalence and outcomes of pulmonary arterial hypertension in advanced idiopathic pulmonary fibrosis. *Chest* 129(3):746–752.
5. Bärtsch P, Gibbs JS (2007) Effect of altitude on the heart and the lungs. *Circulation* 116(19): 2191–2202.
6. Semenza GL (2003) Targeting HIF-1 for cancer therapy. *Nat Rev Cancer* 3(10):721–732.
7. Semenza GL (2009) Regulation of vascularization by hypoxia-inducible factor 1. *Ann N Y Acad Sci* 1177:2–8.
8. Pouysségur J, Dayan F, Mazure NM (2006) Hypoxia signalling in cancer and approaches to enforce tumour regression. *Nature* 441(7092):437–443.
9. Formenti F, et al. (2010) Regulation of human metabolism by hypoxia-inducible factor. *Proc Natl Acad Sci USA* 107(28):12722–12727.
10. Djagaeva I, Doronkin S (2010) Hypoxia response pathway in border cell migration. *Cell Adhes Migr* 4(3):391–395.
11. Hubbi ME, et al. (2014) Cyclin-dependent kinases regulate lysosomal degradation of hypoxia-inducible factor 1α to promote cell-cycle progression. *Proc Natl Acad Sci USA* 111(32): E3325–E3334.
12. Stenmark KR, Meyrick B, Galie N, Mooi WJ, McMurtry IF (2009) Animal models of pulmonary arterial hypertension: The hope for etiological discovery and pharmacological cure. *Am J Physiol Lung Cell Mol Physiol* 297(6):L1013–L1032.
13. Dickinson MG, Bartelds B, Borgdorff MA, Berger RM (2013) The role of disturbed blood flow in the development of pulmonary arterial hypertension: Lessons

from preclinical animal models. *Am J Physiol Lung Cell Mol Physiol* 305(1): L1–L14.
14. Shimoda LA, Manalo DJ, Sham JS, Semenza GL, Sylvester JT (2001) Partial HIF-1alpha deficiency impairs pulmonary arterial myocyte electrophysiological responses to hypoxia. *Am J Physiol Lung Cell Mol Physiol* 281(1):L202–L208.
15. Brusselmans K, et al. (2003) Heterozygous deficiency of hypoxia-inducible factor-2alpha protects mice against pulmonary hypertension and right ventricular dysfunction during prolonged hypoxia. *J Clin Invest* 111(10):1519–1527.
16. Ball MK, et al. (2014) Regulation of hypoxia-induced pulmonary hypertension by vascular smooth muscle hypoxia-inducible factor-1α. *Am J Respir Crit Care Med* 189(3): 314–324.
17. Park SO, et al. (2008) ALK5- and TGFBR2-independent role of ALK1 in the pathogenesis of hereditary hemorrhagic telangiectasia type 2. *Blood* 111(2):633–642.
18. Ryan HE, et al. (2000) Hypoxia-inducible factor-1alpha is a positive factor in solid tumor growth. *Cancer Res* 60(15):4010–4015.
19. Gruber M, et al. (2007) Acute postnatal ablation of Hif-2alpha results in anemia. *Proc Natl Acad Sci USA* 104(7):2301–2306.
20. Yamataka T, Puri P (1997) Pulmonary artery structural changes in pulmonary hypertension complicating congenital diaphragmatic hernia. *J Pediatr Surg* 32(3):387–390.
21. Melillo G, et al. (1995) A hypoxia-responsive element mediates a novel pathway of activation of the inducible nitric oxide synthase promoter. *J Exp Med* 182(6): 1683–1693.
22. Louis CA, et al. (1998) Distinct arginase isoforms expressed in primary and transformed macrophages: Regulation by oxygen tension. *Am J Physiol* 274(3 Pt 2):R775–R782.
23. Takeda N, et al. (2010) Differential activation and antagonistic function of HIF-alpha isoforms in macrophages are essential for NO homeostasis. *Genes Dev* 24(5):491–501.
24. Cowburn AS, et al. (2013) HIF isoforms in the skin differentially regulate systemic arterial pressure. *Proc Natl Acad Sci USA* 110(43):17570–17575.
25. Branco-Price C, et al. (2012) Endothelial cell HIF-1α and HIF-2α differentially regulate metastatic success. *Cancer Cell* 21(1):52–65.
26. Grasemann H, et al. (2015) Arginase inhibition prevents bleomycin-induced pulmonary hypertension, vascular remodeling, and collagen deposition in neonatal rat lungs. *Am J Physiol Lung Cell Mol Physiol* 308(6):L503–L510.
27. Xu W, et al. (2004) Increased arginase II and decreased NO synthesis in endothelial cells of patients with pulmonary arterial hypertension. *FASEB J* 18(14):1746–1748.
28. Firth AL, Yao W, Remillard CV, Ogawa A, Yuan JX (2010) Upregulation of Oct-4 isoforms in pulmonary artery smooth muscle cells from patients with pulmonary arterial hypertension. *Am J Physiol Lung Cell Mol Physiol* 298(4):L548–L557.
29. Toshner M, et al. (2009) Evidence of dysfunction of endothelial progenitors in pulmonary arterial hypertension. *Am J Respir Crit Care Med* 180(8):780–787.
30. Wang JW, et al. (2013) Analysis of the storage and secretion of von Willebrand factor in blood outgrowth endothelial cells derived from patients with von Willebrand disease. *Blood* 121(14):2762–2772.
31. Toshner M, et al. (2014) Transcript analysis reveals a specific HOX signature associated with positional identity of human endothelial cells. *PLoS One* 9(3):e91334.
32. Chu Y, et al. (2016) Arginase inhibitor attenuates pulmonary artery hypertension induced by hypoxia. *Mol Cell Biochem* 412(1–2):91–99.
33. Yu AY, et al. (1999) Impaired physiological responses to chronic hypoxia in mice partially deficient for hypoxia-inducible factor 1alpha. *J Clin Invest* 103(5):691–696.
34. Dai Z, Li M, Wharton J, Zhu MM, Zhao YY (2016) PHD2 deficiency in endothelial cells and hematopoietic cells induces obliterative vascular remodeling and severe pulmonary arterial hypertension in mice and humans through HIF-2alpha. *Circulation* 133(24):2447–2458.
35. Kapitsinou PP, et al. (2016) The endothelial prolyl-4-hydroxylase domain 2/hypoxia-inducible factor 2 axis regulates pulmonary artery pressure in mice. *Mol Cell Biol* 36(10):1584–1594.
36. Machado RF, et al. (2004) Nitric oxide and pulmonary arterial pressures in pulmonary hypertension. *Free Radic Biol Med* 37(7):1010–1017.
37. Girgis RE, et al. (2005) Decreased exhaled nitric oxide in pulmonary arterial hypertension: Response to bosentan therapy. *Am J Respir Crit Care Med* 172(3):352–357.
38. Kaneko FT, et al. (1998) Biochemical reaction products of nitric oxide as quantitative markers of primary pulmonary hypertension. *Am J Respir Crit Care Med* 158(3):917–923.
39. Budts W, et al. (2000) Aerosol gene transfer with inducible nitric oxide synthase reduces hypoxic pulmonary hypertension and pulmonary vascular remodeling in rats. *Circulation* 102(23):2880–2885.
40. Crosby A, et al. (2011) Praziquantel reverses pulmonary hypertension and vascular remodeling in murine schistosomiasis. *Am J Respir Crit Care Med* 184(4):467–473.
41. Crosby A, et al. (2010) Pulmonary vascular remodeling correlates with lung eggs and cytokines in murine schistosomiasis. *Am J Respir Crit Care Med* 181(3):279–288.
42. Crosby A, et al. (2015) Hepatic shunting of eggs and pulmonary vascular remodeling in Bmpr2(+/-) mice with schistosomiasis. *Am J Respir Crit Care Med* 192(11):1355–1365.
43. Morrell NW, Atochina EN, Morris KG, Danilov SM, Stenmark KR (1995) Angiotensin converting enzyme expression is increased in small pulmonary arteries of rats with hypoxia-induced pulmonary hypertension. *J Clin Invest* 96(4):1823–1833.
44. Ormiston ML, et al. (2015) Generation and culture of blood outgrowth endothelial cells from human peripheral blood. *J Vis Exp* (106):e53384.
45. Zhang C, et al. (2004) Upregulation of vascular arginase in hypertension decreases nitric oxide-mediated dilation of coronary arterioles. *Hypertension* 44(6):935–943.
46. Macías D, Fernández-Agüera MC, Bonilla-Henao V, López-Barneo J (2014) Deletion of the von Hippel-Lindau gene causes sympathoadrenal cell death and impairs chemoreceptor-mediated adaptation to hypoxia. *EMBO Mol Med* 6(12):1577–1592.
47. Le-Dong NN, et al. (2012) Measuring exhaled nitric oxide in animal models: methods and clinical implications. *J Breath Res* 6(4):047001.